

# DDL-MVS: Depth Discontinuity Learning for MVS Networks

Nail Ibrahimli, Hugo Ledoux, Julian Kooij, and Liangliang Nan

Delft University of Technology

{n.ibrahimli, h.ledoux, j.f.p.kooij, liangliang.nan}@tudelft.nl

**Abstract.** Traditional MVS methods have good accuracy but struggle with completeness, while recently developed learning-based multi-view stereo (MVS) techniques have improved completeness except accuracy being compromised. We propose depth discontinuity learning for MVS methods, which further improves accuracy while retaining the completeness of the reconstruction. Our idea is to jointly estimate the depth and boundary maps where the boundary maps are explicitly used for further refinement of the depth maps. We validate our idea and demonstrate that our strategies can be easily integrated into the existing learning-based MVS pipeline where the reconstruction depends on high-quality depth map estimation. Extensive experiments on various datasets show that our method improves reconstruction quality compared to baseline. Experiments also demonstrate that the presented model and strategies have good generalization capabilities. The source code will be available soon.

**Keywords:** Multi-view Stereo, Deep Learning, Depth Discontinuity

## 1 Introduction

Multi-view stereo (MVS) techniques have been widely used to obtain dense 3D reconstruction from images. Traditional MVS techniques extract dense correspondences from multiple calibrated views and generate a dense 3D representation (i.e., point cloud or dense triangle mesh) of the scene. These methods rely on image correspondences in the RGB space, which are sensitive to textureless and non-Lambertian surfaces, and to lighting variations.

Recent developments in deep learning allow the use of learned feature maps instead of directly working on RGB images to build more robust MVS pipelines [44,45,20,6]. By learning feature maps about the objects in the scene, learning-based MVS methods have demonstrated better completeness than traditional methods in reconstructing man-made objects with low texture and non-Lambertian surfaces. The key idea of the recent learning-based MVS methods is to learn the depth map from input images via variations of the 3D cost volume regularization [44,15] or differentiable PatchMatch Stereo [38,10].

Earlier works have shown that range images have small spatial variations except for sparse object discontinuities [17], and that higher-quality depth maps

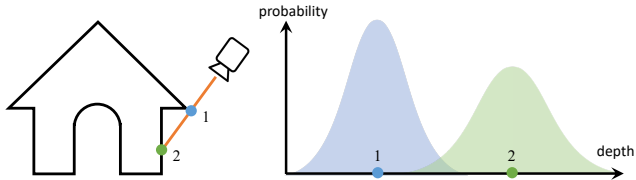


Fig. 1: We propose to estimate depth as a bimodal univariate distribution. Using this depth representation, we improve multi-view depth reconstruction, especially across geometric boundaries.

can be obtained through spatial regularization [3,2]. These works inspire us to learn the geometric edges of the scene objects, instead of the photometric edges. Unlike photometric edges, geometric edges indicate where the object discontinuities truly lie (see Fig. 1). The second-order depth variations (i.e., variations of the changes in depth) are small in smooth surface regions and have large values at boundaries. This motivates us to estimate depth discontinuities by learning to detect the boundaries such that the second-order depth variation is penalized only in the pixels that lie across non-boundary regions.

In the context of depth estimation, transitions between boundaries with depth discontinuities usually cause large noise [51,37]. This kind of noise can be alleviated by post-processing filters, which often damage the completeness of the reconstruction. Our insight into this noise issue is that it is due to building MVS pipelines on pixel-wise depth estimation, especially alongside wrongly inherited smooth surface assumptions around the true boundaries. As illustrated in Fig. 1, it can be ambiguous to determine if a pixel relates to a boundary with large depth discontinuities. Therefore, in this paper, we learn to model the depth as univariate bimodal distribution instead of a single value estimate, this allows us to reduce noise and improve accuracy without compromising completeness. Also, we jointly estimate the geometric boundary maps to get depth maps with smooth surfaces.

Our ideas can be easily integrated into existing learning-based MVS pipelines where a depth map is estimated. Extensive experiments that we ran on various benchmark datasets (see Sect. 4) demonstrate that our method advances the state of the art in terms of completeness. Moreover, our method has high generalization capabilities, which have been validated by training our model on one dataset and testing it on other datasets. In summary, the contributions of this work to multi-view stereo networks are: (1) a novel multi-task learning architecture for joint estimation of depth maps and object boundary maps for learning-based multi-view stereo pipelines; (2) a bimodal depth representation that represents depth as a distribution learned from multi-view images; (3) a general loss formulation for depth discontinuity-based spatial regularization, which helps to learn discontinuities in depth from multiple views and to regularize the depth maps.

## 2 Related work

As learning-based MVS networks are inspired by photogrammetry-based MVS algorithms and developed from two-view methods, we review photogrammetry-based MVS algorithms, learning-based two view methods, and the recent development in learning-based MVS networks.

### 2.1 Photogrammetry-based MVS

Multi-View stereo methods purely built upon photogrammetry and multi-view geometry theory are usually referred to as traditional multi-view stereo methods. Janai et al. [19] showed that the taxonomy of the traditional multi-view stereo methods can be divided into four classes based on their representations of the scene and output. These scene representations are depth maps, point clouds, volumetric representations, and mesh or surfaces.

Volumetric representations use either discrete occupancy function [23], or levelset alike signed distance functions [11], which limits them to small scale reconstruction. The most common mesh-based approaches run variations of the marching cubes algorithm [25] on top of a signed distance function based on a volumetric surface representation [9].

The seminal point cloud-based method PMVS [12] has shown that starting with an initial sparse set of point features it is possible to create an initial set of patches and densify them by iterative greedy expansion and photo-geometric filtering. These methods usually demand a uniformly sampled sparse set of points across the image domain to be able to create point clouds with better completeness.

Depth map-based approaches usually first try to estimate a 2.5D depth map for each view. By using multi-view fusion pipelines [48,9], these depth maps are consolidated into a single geometric model. Although the plane sweeping algorithm [8] has high memory consumption, it was the most commonly used technique for depth map estimation. To use plane sweeping stereo for a large dynamic range of outdoor videos, Pollefeys et al. [30] took advantage of GPS and inertia measurements to place the reconstructed models in geo-registered coordinates. Using random initialization and propagation techniques, the Patch-Match based MVS algorithms [13,33] were able to estimate the depth map of each view with low memory consumption. In this work, we use a differentiable PatchMatch-based module to achieve a similar goal.

### 2.2 Learning-based two-view methods

Learning-based two-view methods have introduced the initial building blocks for two-view stereo matching and depth estimation, which were later adapted for multi-view settings. The most common building blocks for learning-based depth map estimation pipelines are feature extraction and depth estimation from the feature space. Shared weight-based feature extraction was introduced by [49],

and later improved by using cost volume regularization for depth map extraction [21,5,42]. To reduce memory demand of the cost volume, Duggal et al. [10] introduced differentiable PatchMatch Stereo for two-view depth map estimation. These approaches were later adapted for multi-view settings via differentiable homography [5,7,44,38,15].

EdgeStereo [35] uses a pre-trained sub-network for detecting the edges, and the edge cues are then fed into the disparity branch to improve the disparity map. Tosi et al. [37] showed that it is possible to improve the quality of the learning-based two-view stereo networks by integrating an MLP-based bimodal mixture density network. In their work, they improved the accuracy of stereo matching networks [5,42] that were used as a backbone to their mixture density head. Inspired by these works, we also represent depth as bimodal distribution, and we jointly estimate depth maps and object boundary maps in the multi-view stereo setting using a novel multi-task learning architecture. Our pipeline does not involve any parallel (sub)networks and learns directly from multi-view images to estimate edge-depth pairs jointly.

The continuous disparity network [14] aims to regress the multi-modal depth by jointly estimating both probability and offset volume by minimizing a Wasserstein distance between the ground truth and the distribution estimated from the volumes. The offset volume aims to obtain continuous disparity estimations. Our method avoids regressing the offset values and instead, directly estimates bimodal distribution parameters.

### 2.3 Learning-based MVS

State-of-the-art learning-based MVS approaches adapt the photogrammetry-based MVS algorithms by implementing them as a set of differentiable operations defined in the feature space. MVSNet [44] introduced good quality 3D reconstruction by regularizing the cost volume that was computed using differentiable homography on feature maps of the reference and source images. Its network architecture is similar to learning-based two-view stereo matching architecture GCNet [21]. Both MVSNet [44] and GCNet [21] regularize cost volume using a 3D CNN-based U-Net network. The cost volume itself has a very high demand for memory. To circumvent this problem, R-MVSNet uses GRUs [45] to regularize the cost volume sequentially. Follow-up works [15,43], used feature pyramids and cost volume pyramids to learn in a coarse-to-fine manner instead of constructing a cost volume at a fixed resolution. To fully avoid construction of feature cost volume, Wang et. al. [38] introduced a learning-based Multi-View PatchMatch Stereo pipeline. Variations of PatchMatch Stereo are seen as suitable options to work with high-resolution images since both traditional and learning-based Multi-View Patchmatch Stereo avoids the memory demands of Plane Sweep Stereo or feature cost volume regularization.

The recent work of PatchMatchNet [38] showed state-of-the-art results in terms of reconstruction completeness, which is used as a baseline in this work. We use differentiable PatchMatch-based MVS as part of the internal structure of our pipeline. To improve reconstruction quality, we estimate the geometric



boundaries of the scene objects where depth discontinuities lie, and we present a method to regularize the depth map with an estimated boundary map. To our knowledge, our work is the first that uses mixture density networks in a learning-based multi-view stereo pipeline.

### 3 Method

In contrast to existing MVS approaches with depth map representations, in which the depth of each pixel is expressed as a single value, our approach takes advantage of a bimodal depth representation that represents depth as distribution. Our depth map is thus not a common grid of per-pixel scalars, but per-pixel mixture density parameters. The motivation of this module is to implicitly integrate uncertainty notion into our pipeline, which enables us to learn depth discontinuities for spatial regularization of the depth map and to further alleviate the noise gathered in intra-object transitions, foreground-background transitions, and partial occlusions.

The overview of our proposed network architecture is shown in Fig. 2. Our network has three parts, namely, feature extraction, coarse-to-fine PatchMatch Stereo, and depth discontinuity learning, detailed as follows.

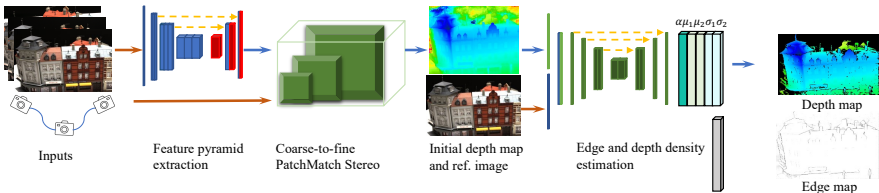


Fig. 2: An overview of the proposed multi-view depth discontinuity learning network that outputs depth and edge information for each pixel. The brown arrows represent input feed and blue arrows represent pipeline flow. We first extract multi-scale features from color images with FPN [24] alike auto-encoder. Then we feed extracted features and camera parameters to the coarse-to-fine PatchMatch stereo module to extract the initial depth map. Using the initial depth map and RGB pair, our network learns bimodal depth parameters and geometric edge maps. We use mixture parameters and photo-geometric filtering to compute our final depth map. The edge map visualized here is negated edge map (for a clear view).

#### 3.1 Feature extraction

We follow the common practice of using feature pyramids to learn features in multiple scales [7,15,43], which also allows us to build our algorithm in a coarse-to-fine regression manner. We adapted the FPN [24] with residual connections

between encoder and decoder, and use three layers of decoder outputs as our extracted features, with each next level having half the resolution of the previous one and the finest level having half dimension (width and height) of the original image. In Fig. 2, the red blocks show three scales of features fed to the coarse-to-fine PatchMatch Stereo module.

### 3.2 Coarse-to-fine PatchMatch Stereo

Following PatchmatchNet [38] that demonstrates good reconstruction completeness and low memory demands, we regress three levels of initial depth maps in a coarse-to-fine manner. We randomly initialize the depth values at the coarsest level, and at a finer level, we initialize the depth values with the outputs of the coarser levels. Following the initialization step, we run an iterative feedback loop between the propagation and evaluation steps. We propagate our estimates with good scoring values to the neighboring pixels. In the evaluation step, we use candidate depth values for differentiable homography warping and matching cost computation.

### 3.3 Depth discontinuity learning

The output of coarse-to-fine PatchMatch Stereo is a conventional depth map of half the resolution (half width and half height) of the original input. Hui et al. [18] showed that a low-resolution depth map can be progressively upsampled with the guidance of the associated high-resolution color image. We follow this idea to bring the depth to the same resolution as the color image.

Unlike other learning-based networks [44,46] that use residual network [16] to refine depth maps, we refine depth maps via learning mixture density parameters and geometric edge maps. Unlike SMD-Nets [37], we use mixture density networks as an internal structure of the depth refinement network and input it with RGB-depth pairs instead of rectified image pairs. Our network learns depth maps alongside boundary maps. We use the same backbone to jointly estimate depth density parameters and boundary maps. In our pipeline, we use a 2D CNN-based U-Net [31] architecture to estimate the bimodal depth density parameters of each pixel in a discrete space. Based on the fact that depth maps have piecewise smoothness and that they can be improved by spatial regularization to smooth regions as shown in earlier works [17,3,2], we propose to refine depth-map quality by learning depth discontinuities.

Previous methods based on pixel-wise single value estimates implicitly balance the depth estimation error between nearby foreground and background pixels for boundary points. Our refinement network regresses the parameters of a bimodal distribution. As suggested by Tosi et al. [37], we use the bimodal Laplacian distribution since it has a sharper shape modality than Gaussian and due to the fact that it optimizes over  $\mathcal{L}_1$  distance instead of  $\mathcal{L}_2$  distance between the groundtruth and estimated mean, to be robust against outliers. The bimodal Laplacian density distribution can be written as

$$\theta = \{\alpha, \mu_1, \sigma_1, \mu_2, \sigma_2\} \quad (1)$$

$$p(x; \theta) = \frac{\alpha}{2\sigma_1} \exp\left(-\frac{|x - \mu_1|}{\sigma_1}\right) + \frac{1 - \alpha}{2\sigma_2} \exp\left(-\frac{|x - \mu_2|}{\sigma_2}\right)$$

where  $\alpha$  is the mixture weight that can be seen as the likeliness of each mode. Later in our work (see Sec. 4), we observe that the network learns to assign different  $\alpha$  values to different scene parts, and in most cases it is binary classifying foreground and background pixels.  $\mu_1$  and  $\mu_2$  are the two depth estimates of the corresponding modes.  $\sigma_1$  and  $\sigma_2$  are the two depth variance measures of each depth value. We also treat  $\frac{\alpha}{\sigma_1}$  and  $\frac{1-\alpha}{\sigma_2}$  as responsibility scores, which aims to determine the responsible mode for the depth of a given pixel. Thus we use a single refinement auto-encoder for three goals: upsampling, refining, multi-task learning.

### 3.4 Depth fusion

For custom data without camera information, we run a standard Structure from Motion (SfM) pipeline [32] to obtain calibrated views. Our proposed architecture outputs the mixture density parameters, which can be used to compute pixel-wise depth values. We treat  $\frac{\alpha}{\sigma_1}$  and  $\frac{1-\alpha}{\sigma_2}$  as responsibility scores where  $\alpha, \sigma_1, \sigma_2$  are estimated mixture parameters. These responsibility scores determine which mode is responsible for the depth of a given pixel. We thus create our final depth map by using the mean  $\mu$  of each pixel’s responsible mode. Following traditional MVS methods [33,13] and learning-based MVS methods [44,38] that run depth map fusion pipeline to integrate the 2.5D depth maps into a point cloud representation, we use the same fusion pipeline that does photometric and geometric consistency checks as in traditional method [29] before accepting a point. After photo-geometric filtering, we obtain a photo-geometrically consistent depth map as shown in Fig. 2.

### 3.5 Loss function

Our loss function has four terms: Depth-groundtruth loss, Edge-depth loss, Smoothness loss, and Bimodal depth loss, each defined with a specific purpose.

**Depth-groundtruth loss.** This loss term measures the difference in depth maps between prediction and the groundtruth. It is defined as the mean absolute error (MAE) of the estimated depth map, i.e.,  $\mathcal{L}_1$  distance between the estimated depth and ground-truth depth across all stages of the PatchMatch Stereo and the final reconstructed depth,

$$L_{gt} = \sum_{k=0}^3 \left[ \frac{1}{N_k} \mathcal{L}_1(D_k, \hat{D}_k) \right], \quad (2)$$

where  $k \in \{0, 1, 2, 3\}$  denotes the scale index of the coarse-to-fine PatchMatch stereo that estimates initial low resolution depth maps, with 0 representing the finest input and output resolution, and from 3 to 1 the coarser-to-finer scales

of the PatchMatch stereo output.  $\hat{D}_k$  and  $D_k$  represent the ground-truth depth map and estimated depth map at resolution level  $k$ , respectively.  $N_k$  represents a number of pixels in each scale.

**Edge-depth loss.** Geometric edges or boundaries are expected where there are depth discontinuities in the depth map. Thus, the edge-depth loss term measures how much the estimated edges agree with the second-order depth variations (i.e., depth discontinuities). It is defined as the mean squared error (MSE) ( $\mathcal{L}_2$  distance) between the estimated edges and groundtruth changes of variations in depth,

$$L_{ed} = \frac{1}{N} \mathcal{L}_2(E, \phi(\Delta \hat{D}, \tau)), \quad (3)$$

where  $\phi$  is the function that takes Laplacian of the depth and threshold value  $\tau$  to return the mask image where the Laplacian response of the depth map is higher than the  $\tau$ .  $N$  denotes the number of pixels. With this term, we explicitly inform the network that we are expecting geometric edges or boundaries at the pixels where there exist depth discontinuities. We calculate depth discontinuities using the Laplacian operator that is the second-order depth change.

**Smoothness loss.** Except for the geometric edges and boundaries with depth discontinuities, real-world objects typically demonstrate piecewise smoothing surfaces. Thus, we would like to encourage local smoothness for the regions without depth discontinuities. We achieve this by introducing an edge-aware smoothness loss term to penalize second-order depth variations in non-boundary regions,

$$L_{sm} = \frac{1}{N} \sum_{i \in \Omega} \omega(E_i) |\Delta D_i|, \quad (4)$$

$$\omega(E_i) = \exp(-\beta E_i)$$

where  $E_i$  will have a value close to 1 for boundaries and close to 0 for non-boundary pixels.  $\omega$  is a weight function that plays a role of a switch, which returns a value close to 0 for boundaries and close to 1 for non-boundary pixels. Thus, second-order depth change in non-boundary regions contributes to our smoothness loss.  $\beta$  is a tunable hyper-parameter that controls the sharpness of change in the  $\omega$  function.  $N$  denotes the number of the pixels in the image space  $\Omega$ . To the best of our knowledge, this is the first time depth discontinuities are explicitly learned and used for spatial regularization in multi-view stereo networks.

**Bimodal loss.** Following the work of SMD-Nets [37], we compute the negative-log-likelihood of the distribution as a bimodal loss term, i.e.,

$$L_{bi} = \frac{1}{N} \sum_{i \in \Omega} -\log(p(\hat{D}_i; \theta, i)), \quad (5)$$

where  $\hat{D}_i$  represent the groundtruth depth measured at pixel  $i$ , and  $\theta$  is the parameter of the bimodal distribution introduced in Eq. 1.

**Total loss.** We simply use the weighted sum of the aforementioned loss terms

$$L_{total} = L_{gt} + \lambda_1 L_{ed} + \lambda_2 L_{sm} + \lambda_3 L_{bi} \quad (6)$$

as a training criterion for our network to optimize the parameters via backpropagation.  $\lambda_1 = 4$ ,  $\lambda_2 = 1.25$ , and  $\lambda_3 = 0.5$ , are hyper-parameters empirically set based on our experiments on the validation set.

## 4 Experiments and Evaluation

We have tested and evaluated our method on multiple datasets: the small baseline dataset DTU [1], and the large baseline datasets “Tanks and Temples” [22] and ETH3D [34]. We used the same model to quantitatively evaluate the generalization capabilities of our method and to compare it with other methods. All the metric results of the other methods were collected from the corresponding papers, and the 3D point clouds of other papers were reconstructed using the code and pre-trained models provided by the authors. For a fair comparison, all methods were trained using the same dataset.

Fig. 3 demonstrates some of our visual results (i.e., point clouds) and the visual comparison with the baseline method PatchmatchNet [38]. We can observe that our results show better completeness and are cleaner, especially for the indoor scenes with low textures.

### 4.1 Evaluation on DTU dataset

The DTU dataset [1] is a benchmark with 124 scenes captured by a structured-light sensor under seven different lighting conditions. It has been widely used for developing learning-based MVS methods and evaluating their performance in terms of completeness and accuracy. Following this benchmark, we recorded the *accuracy*, *completeness*, and *overall* performance metrics of our method, and compared them to other methods. The *accuracy* is measured as the mean error distance between the closest points from the reconstruction to the structured-light reference. *completeness* is measured as the mean error distance between the closest points from the reference to the reconstruction, and *overall* is the algebraic mean of *accuracy* and *completeness*. Therefore having lower metric scores is better for this benchmark.

The result on the DTU dataset is reported in Tab. 1. From the result, we can see that traditional photogrammetry-based methods generally have better accuracy, while learning-based methods have better completeness and *overall* performance. Furthermore, it also reveals that the *completeness* gap between learning-based and photogrammetry-based methods are bigger than their gap in *accuracy*, which motivated us to use a coarse-to-fine PatchMatch Stereo to build our initial depth estimation block, to reduce the *accuracy* gap while still improving completeness. Compared with the state-of-the-art leaning-based MVS methods, our method demonstrates better *completeness* and *overall* scores. This reveals that learning depth discontinuities is an effective means to improve both reconstruction accuracy and completeness.

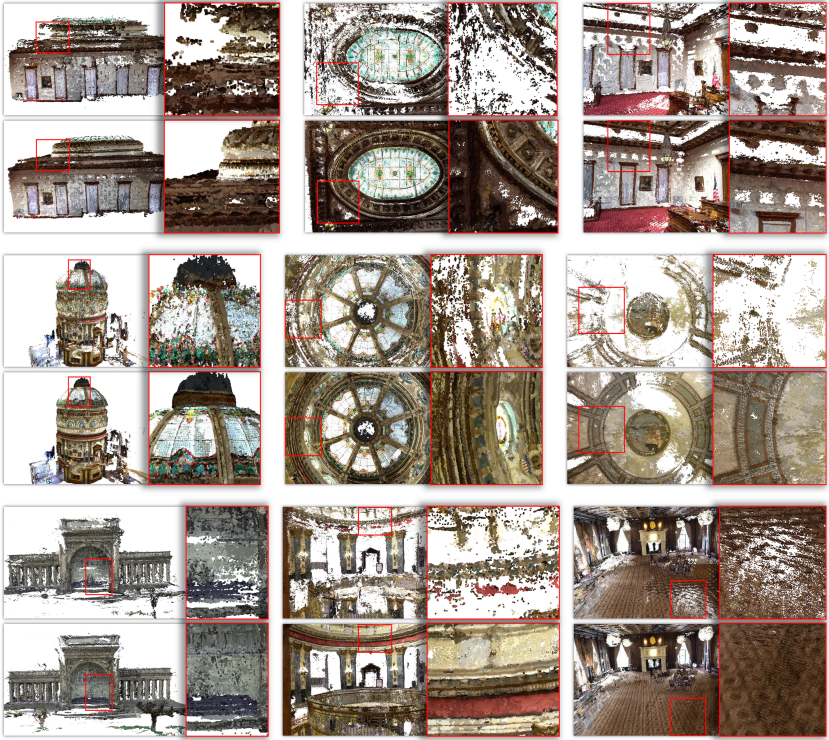


Fig. 3: Comparison between our method and the baseline method PatchmatchNet [38] on a set of scenes from the Tanks and Temples dataset [22]. For each scene, the top row shows the results from PatchmatchNet, and the bottom row shows the results from our method. A zoomed view of the marked image region is shown on the right of each result.

## 4.2 Evaluation on “Tanks and Temples” dataset

“Tanks and Temples” is a real-world large-scale dataset consisting of both indoor and outdoor scenes [22]. It has two parts: an intermediate set consisting of images of sculptures, large vehicles, and house-scale buildings (taken from the exterior), and an advanced set consisting of images of large indoor scenes and large outdoor scenes with complex geometric layouts and repetitive structures. This benchmark has three metrics, namely, recall, precision, and F-score. Recall and precision represent the completeness and accuracy of the reconstruction, respectively, both measured in percentage (%). The F-score combines precision and recall, and it is defined as the harmonic mean of a model’s precision and recall.

In our experiments, we used our model trained using the DTU dataset with 14 epochs with all the proposed loss terms. We compared the results against those from our baseline method PatchmatchNet [38]. For both methods, we ran the same depth map fusion algorithm with the same threshold value to not to

Method	Accuracy ( <i>mm</i> )	Completeness ( <i>mm</i> )	Overall ( <i>mm</i> )
Traditional photogrammetry-based			
Camp [4]	0.835	0.554	0.695
Furu [12]	0.613	0.941	0.777
Tola [36]	0.342	1.190	0.766
Gipuma [13]	<b>0.283</b>	0.873	0.578
Learning-based			
SurfaceNet [20]	0.450	1.040	0.745
MVSNet [44]	0.396	0.527	0.462
R-MVSNet [45]	0.383	0.452	0.417
CIDER [41]	0.417	0.437	0.427
P-MVSNet [26]	0.406	0.434	0.420
Point-MVSNet [6]	0.342	0.411	0.376
AttMVS [27]	0.383	0.329	0.356
Fast-MVSNet [47]	0.336	0.403	0.370
Vis-MVSNet [50]	0.369	0.361	0.365
CasMVSNet [15]	0.325	0.385	0.355
UCS-Net [7]	0.338	0.349	0.344
EPP-MVSNet [28]	0.413	0.296	0.355
CVP-MVSNet [43]	0.296	0.406	0.351
AA-RMVSNet [39]	0.376	0.339	0.357
PatchmatchNet [38]	0.427	0.277	0.352
Ours ( $L_{1,4}$ )	0.405	<b>0.267</b>	<b>0.336</b>
Ours ( $L_{1,2,3,4}$ )	0.399	0.280	<b>0.339</b>

Table 1: Quantitative comparison with photogrammetry-based and learning-based MVS methods, on the DTU dataset [1]. Two different settings (with different loss functions) of our method were tested.  $L_1$ : depth-groundtruth loss;  $L_2$ : edge-depth loss;  $L_3$ : smoothness loss;  $L_4$ : bimodal loss. Please note that the metrics are error-based and thus the smaller the better.

gain any advantage in the evaluation process. As can be seen from the statistics reported in Tab. 3, our results on the intermediate set have better performance on all evaluation metrics. On the advanced set, our results demonstrate better accuracy and F-score, and the results from PatchmatchNet have slightly better completeness. For qualitative results and comparison, please refer to Fig. 3.

### 4.3 Evaluation on ETH3D dataset

The ETH3D benchmark [34] consists of high-resolution images of scenes with sparse scene coverage, high viewpoint variation, and camera parameter information. The quantitative evaluation of our method and the comparison with PatchmatchNet [38] on the ETH3D dataset [34] are detailed in Tab. 2. Both methods have used the same fusion pipeline. Our method demonstrates better accuracy and F-score, while PatchmatchNet has better completeness.

Method	Accuracy (%)	Completeness (%)	F-score
PatchmatchNet	64.81	<b>65.43</b>	64.21
Ours	<b>64.96</b>	65.21	<b>64.37</b>

Table 2: Quantitative evaluation of our method and comparison with PatchmatchNet [38] on the ETH3D training set [34]. Following the benchmark, the *accuracy* and *completeness* measures are quantified using the percentage of points below a 2 *cm* error margin (the higher the better).

Methods	Intermediate set			Advanced set		
	P (%)	R (%)	F-score	P (%)	R (%)	F-score
PatchmatchNet	43.64	69.38	53.15	27.27	<b>41.66</b>	32.31
Ours	<b>45.12</b>	<b>69.69</b>	<b>54.30</b>	<b>28.31</b>	41.06	<b>32.80</b>

Table 3: Evaluation and comparison with PatchmatchNet [38] on the “Tanks and Temples” dataset [22].

Methods	Point clouds (testing)			Depth maps (validation)	
	Acc. ( <i>mm</i> )	Comp. ( <i>mm</i> )	Overall ( <i>mm</i> )	Depth map ( <i>mm</i> )	Error ratio (%; error > 8 <i>mm</i> )
PatchmatchNet [38]	0.427	0.277	0.352	7.33	11.68
Architecture + $L_1$	0.412	0.273	0.342	5.41	9.07
Architecture + $L_{1,2,3}$	0.412	0.270	0.341	5.44	8.96
Architecture + $L_{1,4}$	0.405	<b>0.267</b>	<b>0.336</b>	5.47	9.01
Architecture + $L_{1,2,3,4}$	<b>0.399</b>	0.280	0.339	<b>5.31</b>	<b>8.91</b>

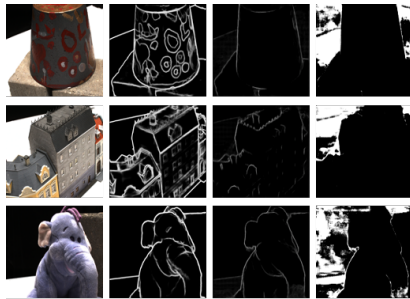
Table 4: Ablation study on the point clouds and depth maps from the DTU dataset [1].  $L_1$ : depth-groundtruth loss;  $L_2$ : edge-depth loss;  $L_3$ : smoothness loss;  $L_4$ : bimodal loss. Note that  $L_2$  and  $L_3$  cannot be separated because they together work for edge-aware smoothness.

#### 4.4 Ablation study

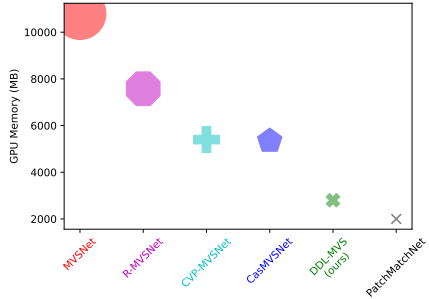
We have conducted an ablation study to understand and analyze the contributions of the aforementioned loss terms of our architecture. The results are detailed in Tab. 4. Since the edge-depth loss and the smoothness loss terms together strive for edge-aware smoothness, we do not separate them in our experiments. We retrieve the last two metrics from the validation set while tuning our hyperparameters. The “Depth map” represents the accuracy of the estimated depth map, calculated using mean absolute error (MAE) between the estimated depth map and groundtruth. “Error > 8 *mm*” represents the percentage of points in the depth map having the higher error than 8 *mm*.

From Tab. 4, we can see that using all lost terms improves the depth map quality on the validation set. For testing, we observe that our point clouds have better completeness and overall metrics with bimodal and depth ground-truth loss while having edge-aware smoothness term results in better accuracy. Our





(a) Edge maps



(b) GPU memory consumption

Fig. 4: Edges maps and GPU Memory consumption. (a) Edges maps of a few randomly chosen examples. For each example, the images from left to right are color image, edge map predicted by HED [40], our learned edge map, and the  $\alpha$  map, respectively. We can clearly see that our learned edge maps better capture the depth discontinuities, regardless of the photometric changes. It is also interesting to observe that our  $\alpha$  maps distinguish between foreground and background. (b) Comparison of GPU memory demands with existing learning-based MVS networks on DTU dataset with image size  $1152 \times 864$ .

network also improves arithmetic mean of accuracy and completeness if we compare it against the baseline.

#### 4.5 Effect of depth discontinuity learning

From the above experiments and evaluation, our method demonstrates superior reconstruction quality in terms of *completeness* and *overall* quality, which benefits from our depth discontinuity learning. To understand the role of depth discontinuity learning in reconstruction, we visualize the learned depth discontinuities (denoted as edge maps) for a few randomly picked examples in Fig. 4 (a), and compare them with the edge maps predicted using the seminal learning-based edge detection method HED [40]. We can see that by learning depth discontinuities, our network can retrieve edges where the true depth discontinuities lie. Thus, as a key component for learning-based MVS pipelines, our discontinuity-aware depth learning is more robust to photometrical changes, shadows, and small variations in depth. In the earlier stage of the development of DDL-MVS, we tried to feed the network with HED [40] output and jointly refine the depth and edge maps similar to EdgeStereo [35]. It turned out that even after refinement, the edges were too sensitive to photometric changes, leading to higher depth errors.

To reveal how our depth discontinuity learning contributes to depth estimation, we demonstrate the  $\alpha$  map of each example in the last column of Fig. 4 (a), where  $\alpha$  is the mixture weight in the bimodal Laplacian density distribution (see Eq. 1). It is surprisingly interesting to observe that our network tries to

learn to differentiate foreground and background, for which the  $\alpha$  values express a binary classification for foreground and background pixels.

#### 4.6 Memory consumption and running times

In Fig. 4, we report our comparison of GPU memory demands with existing learning-based MVS networks on the DTU dataset [1], from which we can see that the memory demand of our network is much lower than most of the existing networks. On the DTU dataset with the default parameters and the 5-view case, the average depth inference time for our model is  $345ms$ , which is comparable to the most efficient model of PatchmatchNet [38] (which took  $300ms$ ). We used a dual GPU of NVIDIA GeForce RTX 2080 for the experiments.

#### 4.7 Limitations

Although our method has good completeness and a good overall score (see Tab. 1), it has still not reached the accuracy level of traditional photogrammetry-based algorithms such as Gipuma [13], which is a common weakness in recently developed learning-based MVS methods. There is usually a trade-off between accuracy and completeness since increasing completeness also means increasing the potential source of the noise. Although using bimodality helps to reduce the noise, we observe that our work, like other traditional and learning-based algorithms, contains noise, especially in sparsely viewed regions that may need further research. It is also worth noting that in this work we have used the same fusion pipeline as in other papers [38,44]. Increasing the accuracy and keeping the completeness by compromising point density is certainly favorable.

### 5 Conclusion

We have presented a strategy for improving MVS networks by learning depth discontinuities. Our experiments have shown that learning depth maps implicitly as a mixture distribution can improve reconstruction quality. Learning depth discontinuities and integrating them to the network as a means of prior knowledge for piecewise smoothness regularization improves the accuracy alongside keeping good completeness of the final reconstruction. On large datasets with good view coverage, we have noticed that our network excels to generate more points that successfully pass the geometric and photometric filters of the fusion algorithm, which contributes to better completeness and overall better geometry. As future work, we plan to investigate the foreground and background transitions and learn these transitions via the means of probabilistic framework and multi-modal distribution.

### References

1. Aanæs, H., Jensen, R.R., Vogiatzis, G., Tola, E., Dahl, A.B.: Large-scale data for multiple-view stereopsis. *International Journal of Computer Vision* pp. 1–16 (2016)

2. Boykov, Y., Veksler, O., Zabih, R.: Markov random fields with efficient approximations. In: Proceedings. 1998 IEEE Computer Society Conference on Computer Vision and Pattern Recognition (Cat. No.98CB36231). pp. 648–655 (1998). <https://doi.org/10.1109/CVPR.1998.698673>
3. Boykov, Y., Veksler, O., Zabih, R.: Fast approximate energy minimization via graph cuts. *IEEE Transactions on pattern analysis and machine intelligence* **23**(11), 1222–1239 (2001)
4. Campbell, N.D.F., Vogiatzis, G., Hernández, C., Cipolla, R.: Using multiple hypotheses to improve depth-maps for multi-view stereo. In: Forsyth, D., Torr, P., Zisserman, A. (eds.) *Computer Vision – ECCV 2008*. pp. 766–779. Springer Berlin Heidelberg, Berlin, Heidelberg (2008)
5. Chang, J.R., Chen, Y.S.: Pyramid stereo matching network. In: Proceedings of the IEEE Conference on Computer Vision and Pattern Recognition. pp. 5410–5418 (2018)
6. Chen, R., Han, S., Xu, J., Su, H.: Point-based multi-view stereo network. In: The IEEE International Conference on Computer Vision (ICCV) (2019)
7. Cheng, S., Xu, Z., Zhu, S., Li, Z., Li, L.E., Ramamoorthi, R., Su, H.: Deep stereo using adaptive thin volume representation with uncertainty awareness. In: Proceedings of the IEEE/CVF Conference on Computer Vision and Pattern Recognition. pp. 2524–2534 (2020)
8. Collins, R.T.: A space-sweep approach to true multi-image matching. In: Proceedings CVPR IEEE Computer Society Conference on Computer Vision and Pattern Recognition. pp. 358–363. IEEE (1996)
9. Curless, B., Levoy, M.: A volumetric method for building complex models from range images. In: Proceedings of the 23rd annual conference on Computer graphics and interactive techniques. pp. 303–312 (1996)
10. Duggal, S., Wang, S., Ma, W.C., Hu, R., Urtasun, R.: Deeppruner: Learning efficient stereo matching via differentiable patchmatch. In: ICCV (2019)
11. Faugeras, O., Keriven, R.: Variational principles, surface evolution, PDE’s, level set methods and the stereo problem. *IEEE* (2002)
12. Furukawa, Y., Ponce, J.: Accurate, dense, and robust multi-view stereopsis **32**(8), 1362–1376 (2010)
13. Galliani, S., Lasinger, K., Schindler, K.: Massively parallel multiview stereopsis by surface normal diffusion (June 2015)
14. Garg, D., Wang, Y., Hariharan, B., Campbell, M., Weinberger, K.Q., Chao, W.L.: Wasserstein distances for stereo disparity estimation. *arXiv preprint arXiv:2007.03085* (2020)
15. Gu, X., Fan, Z., Zhu, S., Dai, Z., Tan, F., Tan, P.: Cascade cost volume for high-resolution multi-view stereo and stereo matching (2019)
16. He, K., Zhang, X., Ren, S., Sun, J.: Deep residual learning for image recognition. In: Proceedings of the IEEE conference on computer vision and pattern recognition. pp. 770–778 (2016)
17. Huang, J., Lee, A., Mumford, D.: Statistics of range images. In: Proceedings IEEE Conference on Computer Vision and Pattern Recognition. CVPR 2000 (Cat. No.PR00662). vol. 1, pp. 324–331 vol.1 (2000). <https://doi.org/10.1109/CVPR.2000.855836>
18. Hui, T.W., Loy, C.C., Tang, X.: Depth map super-resolution by deep multi-scale guidance. In: Proceedings of European Conference on Computer Vision (ECCV) (2016)

19. Janai, J., Güney, F., Behl, A., Geiger, A., et al.: Computer vision for autonomous vehicles: Problems, datasets and state of the art. *Foundations and Trends® in Computer Graphics and Vision* **12**(1–3), 1–308 (2020)
20. Ji, M., Gall, J., Zheng, H., Liu, Y., Fang, L.: SurfaceNet: an end-to-end 3d neural network for multiview stereopsis (2017)
21. Kendall, A., Martirosyan, H., Dasgupta, S., Henry, P., Kennedy, R., Bachrach, A., Bry, A.: End-to-end learning of geometry and context for deep stereo regression. In: *Proceedings of the IEEE International Conference on Computer Vision*. pp. 66–75 (2017)
22. Knapitsch, A., Park, J., Zhou, Q.Y., Koltun, V.: Tanks and temples: Benchmarking large-scale scene reconstruction. *ACM Transactions on Graphics* **36**(4) (2017)
23. Kutulakos, K.N., Seitz, S.M.: A theory of shape by space carving. *International journal of computer vision* **38**(3), 199–218 (2000)
24. Lin, T.Y., Dollár, P., Girshick, R., He, K., Hariharan, B., Belongie, S.: Feature pyramid networks for object detection. In: *Proceedings of the IEEE conference on computer vision and pattern recognition*. pp. 2117–2125 (2017)
25. Lorensen, W.E., Cline, H.E.: Marching cubes: A high resolution 3d surface construction algorithm. *ACM siggraph computer graphics* **21**(4), 163–169 (1987)
26. Luo, K., Guan, T., Ju, L., Huang, H., Luo, Y.: P-mvsnet: Learning patch-wise matching confidence aggregation for multi-view stereo. In: *2019 IEEE/CVF International Conference on Computer Vision (ICCV)*. pp. 10451–10460 (2019). <https://doi.org/10.1109/ICCV.2019.01055>
27. Luo, K., Guan, T., Ju, L., Wang, Y., Chen, Z., Luo, Y.: Attention-aware multi-view stereo. In: *Proceedings of the IEEE/CVF Conference on Computer Vision and Pattern Recognition (CVPR)* (June 2020)
28. Ma, X., Gong, Y., Wang, Q., Huang, J., Chen, L., Yu, F.: Epp-mvsnet: Epipolar-assembling based depth prediction for multi-view stereo. In: *Proceedings of the IEEE/CVF International Conference on Computer Vision*. pp. 5732–5740 (2021)
29. Merrell, P., Akbarzadeh, A., Wang, L., Mordohai, P., Frahm, J.M., Yang, R., Nistér, D., Pollefeys, M.: Real-time visibility-based fusion of depth maps. In: *2007 IEEE 11th International Conference on Computer Vision*. pp. 1–8. IEEE (2007)
30. Pollefeys, M., Nistér, D., Frahm, J.M., Akbarzadeh, A., Mordohai, P., Clipp, B., Engels, C., Gallup, D., Kim, S.J., Merrell, P., et al.: Detailed real-time urban 3d reconstruction from video. *International Journal of Computer Vision* **78**(2), 143–167 (2008)
31. Ronneberger, O., Fischer, P., Brox, T.: U-net: Convolutional networks for biomedical image segmentation. *arxiv 2015. arXiv preprint arXiv:1505.04597* (2019)
32. Schönberger, J.L., Frahm, J.M.: Structure-from-motion revisited. In: *Conference on Computer Vision and Pattern Recognition (CVPR)* (2016)
33. Schönberger, J.L., Zheng, E., Pollefeys, M., Frahm, J.M.: Pixelwise view selection for unstructured multi-view stereo. In: *European Conference on Computer Vision (ECCV)* (2016)
34. Schöps, T., Schönberger, J.L., Galliani, S., Sattler, T., Schindler, K., Pollefeys, M., Geiger, A.: A multi-view stereo benchmark with high-resolution images and multi-camera videos. In: *Conference on Computer Vision and Pattern Recognition (CVPR)* (2017)
35. Song, X., Zhao, X., Hu, H., Fang, L.: Edgestereo: A context integrated residual pyramid network for stereo matching. In: *ACCV*. Springer (2018)
36. Tola, E., Strecha, C., Fua, P.: Efficient large-scale multi-view stereo for ultra high-resolution image sets **23**(5), 903–920 (2012)

37. Tosi, F., Liao, Y., Schmitt, C., Geiger, A.: Smd-nets: Stereo mixture density networks. In: Conference on Computer Vision and Pattern Recognition (CVPR) (2021)
38. Wang, F., Galliani, S., Vogel, C., Speciale, P., Pollefeys, M.: Patchmatchnet: Learned multi-view patchmatch stereo (2021)
39. Wei, Z., Zhu, Q., Min, C., Chen, Y., Wang, G.: Aa-rmvsnet: Adaptive aggregation recurrent multi-view stereo network. In: Proceedings of the IEEE/CVF International Conference on Computer Vision. pp. 6187–6196 (2021)
40. Xie, S., Tu, Z.: Holistically-nested edge detection. In: Proceedings of the IEEE international conference on computer vision. pp. 1395–1403 (2015)
41. Xu, Q., Tao, W.: Learning inverse depth regression for multi-view stereo with correlation cost volume. CoRR **abs/1912.11746** (2019), <http://arxiv.org/abs/1912.11746>
42. Yang, G., Manela, J., Happold, M., Ramanan, D.: Hierarchical deep stereo matching on high-resolution images. In: Proceedings of the IEEE/CVF Conference on Computer Vision and Pattern Recognition. pp. 5515–5524 (2019)
43. Yang, J., Mao, W., Alvarez, J.M., Liu, M.: Cost volume pyramid based depth inference for multi-view stereo. In: The IEEE/CVF Conference on Computer Vision and Pattern Recognition (CVPR) (June 2020)
44. Yao, Y., Luo, Z., Li, S., Fang, T., Quan, L.: Mvsnet: Depth inference for unstructured multi-view stereo. European Conference on Computer Vision (ECCV) (2018)
45. Yao, Y., Luo, Z., Li, S., Shen, T., Fang, T., Quan, L.: Recurrent mvsnet for high-resolution multi-view stereo depth inference. Computer Vision and Pattern Recognition (CVPR) (2019)
46. Yu, A., Guo, W., Liu, B., Chen, X., Wang, X., Cao, X., Jiang, B.: Attention aware cost volume pyramid based multi-view stereo network for 3d reconstruction. ISPRS Journal of Photogrammetry and Remote Sensing **175**, 448–460 (2021)
47. Yu, Z., Gao, S.: Fast-mvsnet: Sparse-to-dense multi-view stereo with learned propagation and gauss-newton refinement. In: CVPR (2020)
48. Zach, C., Pock, T., Bischof, H.: A globally optimal algorithm for robust tv-l 1 range image integration. In: 2007 IEEE 11th International Conference on Computer Vision. pp. 1–8. IEEE (2007)
49. Zbontar, J., LeCun, Y., et al.: Stereo matching by training a convolutional neural network to compare image patches. J. Mach. Learn. Res. **17**(1), 2287–2318 (2016)
50. Zhang, J., Yao, Y., Li, S., Luo, Z., Fang, T.: Visibility-aware multi-view stereo network. British Machine Vision Conference (BMVC) (2020)
51. Zhu, S., Brazil, G., Liu, X.: The edge of depth: Explicit constraints between segmentation and depth. In: Proceedings of the IEEE/CVF Conference on Computer Vision and Pattern Recognition. pp. 13116–13125 (2020)